

CFD-based comfort parameter evaluation of a flow vectoring air vent system for car cabins using a reduced order model

S. Langhorst^{1,3}, M. Mrosek¹, N. Boughanmi¹, D. Schmeling², C. Wagner^{2,3}

¹ Volkswagen AG, Group Innovation, Wolfsburg, Germany

² German Aerospace Center (DLR), Institute of Aerodynamics and Flow Technology, Göttingen, Germany

³ TU Ilmenau, Faculty of Mechanical Engineering, Department of Aerodynamics, Ilmenau, Germany

Keywords: Passenger car cabin, Air vent, Volume flow vectoring, Computational fluid dynamics (CFD), Reduced order model (ROM)

Abstract

This Computational Fluid Dynamics (CFD) study examines the comfort parameters of an innovative air vent concept for car cabin interiors using a Reduced Order Model (ROM) and Proper Orthogonal Decomposition (POD). The focus is on the analysis of the influence of geometric and fluid mechanical parameters on the resulting jet, in particular on the deflection angle of the airflow and the total pressure difference along the outlet geometry. Different parameters of the investigated system, such as the surface orientation, the outlet height, the separator distance and the separator height, lead to different effects on the airflow structure. The results show that changes in the air vent surface orientation are always accompanied by an increase in the deflection angle and the total pressure difference. In contrast, the variation of the outlet height ratio positively influences the deflection angle and the total pressure difference in terms of the requirements for air vent geometries. The study also examines the interaction of the geometric parameters and reveals complex correlations which influence the resulting air jet. A comprehensive understanding of these influences makes it possible to adapt the design and implementation of new and innovative air vent concepts to meet specific requirements. By balancing design considerations and technical requirements, optimized solutions are characterized by a high deflection angle and a reduced overall pressure difference for improved system performance and efficiency. Therefore, this evaluation provides a final framework for the design and implementation of an innovative air vent concept based on the volume flow vectoring that is tailored to specific application requirements.

Introduction

The interior of novel electric vehicles is subject to the growing interest in design and new technological developments - with passenger comfort and efficiency playing a key role [1]. The perceived design quality and the range of electric vehicles have a significant influence on the purchase decision. Therefore, a balance between complexity and uniformity in design with reduced technical development requirements is of great interest [2]. In this area of tension, customized

passenger compartment ventilation plays an important role. According to Baker et al. [3], this design-centric view can lead to an incorrect layout of air ducts, misplaced passenger air outlets and a system with high pressure loss. An analysis of the A2Mac1 automotive benchmarking database [4], which includes 902 air vents, shows that manual adjustment of the grid vanes is preferred in current models. The advantages include low pressure losses in the ventilation system and sufficient adjustability of the air jet. However, the lack of concealable design and space makes integration into future vehicle concepts more difficult. Innovative ventilation concepts without visible adjustment elements and small cross-sectional ratios (aspect ratio of air outlet height to width less than or equal to 1:5) must be developed to fulfill the requirements for conventional grid vane air vents described in [5,6]. These requirements – especially the deflection angle of the airflow – are crucial to ensure optimal comfort conditions. Efficient ventilation and consequently low pressure loss due to the air outlet geometry play a central role here, as air conditioning has a significant influence on the overall energy balance and thus on the range of electric vehicles. New air vents for automotive interior concepts must therefore offer a balanced solution to meet design, comfort and energy efficiency requirements. An extensive patent search, carried out as preliminary work in the field of innovative air vent concepts for car cabin interiors, revealed a viable functional principle. The concept of volume flow vectoring, first described in the patent by Yada and Ito [7] as well as in the patent by Othmer [8], and others, offers a promising air outlet geometry with small cross-sectional ratios. So far, however, a systematic flow analysis of this innovative air vent concept has not been carried out in order to ensure a customized design of the vehicle interior without technical restrictions. The present analysis clarifies the correlation between the geometric and flow characteristics of the air vent, the resulting jet and the efficiency of the system. To evaluate the operation and functionality of this selected air vent concept with low aspect ratio, it is necessary to vary various geometric and fluid mechanical parameters to avoid potential comfort or efficiency issues.

The design and construction of prototypes for an experimental flow investigation is expensive and time-consuming. Therefore, numerical studies are essential to develop and understand the flow structure of

the resulting air jet. The current time scales for flow comparisons using Computational Fluid Dynamics (CFD) do not allow all possible geometric and fluid mechanical configurations to be evaluated. This limitation entails an increase in the number of intermediate variation steps to minimize the number of computations, which can lead to an incomplete resulting analysis. This study presents the application and advantages of an implemented Design of Experiments (DoE) approach in combination with a Reduced Order Model (ROM) based on Proper Orthogonal Decomposition (POD) for an air vent geometry based on volume flow vectoring. Similar POD procedures in the area of passenger comfort in a vehicle interior are presented in the studies on the simulation of the air temperature in a car cabin [9], on the optimization of an air outlet concept in a commercial aircraft [10,11] and on the investigation of a mixing cavity in a car heating, ventilating, and air-conditioning model [12]. The approach for the present study is implemented and used for a case in aerodynamics by Mrosek et al. [13] for a time-efficient analysis of a large parameter domain. This approach makes it possible to perform numerical flow analyses for all possible geometric configurations in combination with different fluid mechanical boundary conditions in the defined parameter domain. The goal is to better understand the influence of the geometric and fluid mechanical parameters on the flow entering the car cabin through air outlets. In addition, an optimized air outlet geometry providing the largest possible flow deflection angle for the lowest total pressure difference for specific geometrical design restrictions is to be determined.

Test Case and Parameter Domain

A schematic representation of the studied air vent geometry, which is based on the concept of volume flow vectoring, is shown in *Figure 1*. The adjustability of the air jet is based on the separation of the main volume flow into two partial volume flows, \dot{V}_1 and \dot{V}_2 , with the resulting mean air velocities u_1 and u_2 . A central separator with the height h_3 is required to produce two individual jets. If the separation distance l is greater than zero, the converging and merging zone for the two basic jets, \dot{V}_1 and \dot{V}_2 , is located within the air outlet geometry. If l is zero, the current air jets merge completely outside of the outlet. The height of the air outlet is defined by the variable h_4 , the surface orientation, with respect to the horizontal x -axis, by β . The geometric parameter h_4 is crucial for the design and integration into the passenger compartment concept, as this dimension reflects the area of the air vents visible to the occupants. The deflection angle α of the resulting total volume flow \dot{V}_{total} , with respect to the x -axis and the point of origin in the center of the air outlet, can be adjusted by varying the momentum of the individual jets \dot{V}_1 and \dot{V}_2 . Therefore, this air vent concept deflects the resulting jet without any visible adjustment elements. Given the same physical specifications, such as temperature, density, and the identical flow uniformity of both jets, the controllability of the combined air jet is defined by the velocities u_1 and u_2 . Therefore, the flow distribution

$$\mathbf{m} = \mathbf{u}_2 * [\mathbf{u}_1 + \mathbf{u}_2]^{-1} \quad (1)$$

describes the setting of this operating principle, and the implemented volume flows can be specified by the volume rates. For clarity, please refer to the following section, where more detailed deflection configurations for $m = 0.5$, $m = 0.75$ and $m = 1.0$ are visualized in the contour plots in *Figure 2*.

The purpose of this study is to determine the influence of different geometric nozzle dimensions on the resulting deflection angle α of the air jet and on the total pressure difference Δp of the air vent. The

pressure is determined upstream of the air outlet and set in comparison to the ambient pressure. The ideal air vent geometry offers a wide range for adjusting the deflection angle and a low pressure drop. The duct heights h_1 and h_2 are constant and equal to 15 mm in the studied diffuser geometry. All other distance parameters are standardized to h_1 . The modifications of the parameter range are listed in *Table 1* and define a four-dimensional geometric and a two-dimensional flow-related parameterization of the air outlet geometry. The investigation effort generated by this domain is shown as an example of the stepwise variation of the defined parameters in *Table 1*. Varying the distances in steps of 1 mm and the surface orientation in steps of 1° and generating all combinations would result in 426'006 geometric configurations. Varying the fluid mechanical parameters m in steps of 0.1 and \dot{V}_{total} in steps of $10 \text{ m}^3\text{h}^{-1}$ would result in 36 different boundary conditions. The parameter range of the air outlet geometry (see *Table 1*) to be investigated in this study, would require over 15 million numerical simulations for a holistic stepwise investigation. Therefore, it is essential to avoid a stepwise analysis of the influence of the geometric and flow parameters on the variables of interest. The DoE approach used for this purpose in combination with a ROM method based on a relatively small number of numerical flow simulations will be described in the following section.

Methods

Design of Experiment (DoE) to sample the parameter domain

The parameter domain in *Table 1* defined in the previous section was scanned using 200 sampling points. A Latin hypercube sampling scheme was used to obtain the most uniform coverage of the parameter domain. This results in an even distribution of the respective parameter sequences over the entire domain. The applied ROM approach requires the resulting airflow velocity and pressure fields to be defined on topologically equivalent meshes. Therefore, a setup in the ANSA® program was automated to ensure the generation of the 200 meshes required for the numerical flow simulation by morphing a base surface geometry. This allows meshes of identical size and connectivity to be created.

Numerical setup for the air jet analysis

The CFD method used to perform the 200 numerical simulations discussed in the following section is based on the OpenFOAM® library and has been validated in a previous study [14] on the airflow distribution in conventional air vents in a car interior using Particle Image Velocimetry (PIV). As in Lizal et al. [6], the flow analysis to study the direct flow ventilation described in this paper is stationary and isothermal. The 2D air outlet geometry shown in *Figure 1* was meshed with a hybrid grid consisting of 412'000 hexa and 1'400 tetra elements for the numerical simulation. Six wall layers were used in the mesh generation to ensure that the average y^+ value was lower than one. The Reynolds-averaged Navier-Stokes (RANS) equations were solved using the OpenFOAM's steady-state solver simpleFoam together with the shear stress transport (SST) $k-\omega$ turbulence model, as recommended by Heider et al. [15] and You et al. [16] and validated in [14] for such induced jet flows. The two volume flows \dot{V}_1 and \dot{V}_2 were defined at the inlet of the geometry using a uniform bulk flow along each channel height. The outlet boundary condition was specified with a zero gradient for the airflow velocity and a fixed value for the pressure. All the other wall boundaries had a no-slip boundary condition. The initial values within the flow region for the kinetic energy k , the specific dissipation rate ω and the eddy viscosity ν_t were estimated in accordance with Jaramillo et al. [17]. Convergence of the

performed simulations was achieved as soon as the dimensionless residuals for the continuity, velocity and pressure components less than 10^{-3} . Using 128 CPUs on a cluster, the average physical calculation time for the 200 isothermal flow simulations was 15 minutes (standard deviation ± 2 minutes). The resulting flow-related data sets of each calculation contain the main structures of the averaged velocity and pressure fields as well as the scalar quantities α and Δp . The deflection angle α was determined based on the maximum values of the velocity profiles along the jet of the main flow. The listed flow-related data provide the substructure for the advanced ROM setup. All other flow results of the possible air vent configurations, that are not determined by the 200 calculations, are determined using the ROM approach.

Reduced Order Model (ROM) for complete data analysis

This research is based on the preliminary work of Mrosek et al. [13] and represents a feasibility study for a further possible application in the automotive development process. For the complete analysis of the parameter domain a combination of Proper Orthogonal Decomposition + Interpolation (POD+I), as described by Braconnier et al. [18], and Kriging interpolation of the base coefficients, as described by Forrester et al. [19], was used as the model reduction method. POD+I is a data-driven approach, which is why the 200 numerical calculations are provided as training data. For the prediction of all data fields, an in-depth analysis of the truncated POD base was performed. This analysis involves the individual interpolation of the basis coefficients using Kriging models, followed by a linear combination of the reconstructed POD basis vectors to generate a comprehensive prediction for unobserved parameter combinations. Finally, the predictions are refined by scaling with a mean vector to ensure the overall consistency and balance of the prediction result. The approach aims at providing accurate predictions based on existing data and careful analysis of the POD basis vectors. Additional details and information on the systematic implementation of data analysis using a ROM approach can be found in Mrosek et al. [13]. This type of methodology is also used for the optimization of the intake port of a car engine [20] or in aircraft design [21] and further investigated in the study by Karcher [22]. For the present study, this method is used to predict the velocity and pressure fields as well as the scalar target variables α and Δp for all possible geometric and flow-related parameter combinations (see *Table 1*) for the air vent. The workflow was implemented using the NAVPACK ROM toolbox from NAVASTO®. To evaluate the accuracy, the ROM predictions were validated by comparing them to the observed CFD simulations.

Accuracy Analysis

The accuracy analysis begins with a qualitative comparison of the mean air velocity in the x - y -plane for a specific geometric configuration of the air vent. In this case, the selected parameter combination is chosen randomly. For different flow distributions m , the predicted ROM results (*Figures 2a, c and e*) are compared with the calculated CFD results (*Figures 2b, d and f*). It should be noted that the air vent geometry shown in *Figure 2* was not part of the ROM training data. This geometric configuration with the specific flow boundary conditions is suitable for the accuracy analysis, as there are above-average deviations in the scalar result variables, see *Table 2*. *Figure 2a* shows a possible differentiating feature in the velocity fields. When interpolating using the model reduction method, artifacts can occur within the shear layer causing a differentiation of the velocity field. When comparing *Figures 2a and 2b*, a deflection of the air jet can be observed, although the flow distribution at $m = 0.5$ should produce a horizontally oriented airflow. The deviations also have an

effect on the pressure difference Δp , see *Table 2*. When comparing other ROM results that show smaller geometric changes to the base geometry of the morphing process, it can be seen that these deviations can be reduced by smaller cell spacing and the resulting improved morphing. The flow distribution $m = 0.75$ shows a good qualitative and quantitative agreement in *Figures 2c and 2d*. This excellent agreement of the velocity distribution in the near field of the air outlet is also reflected by the values in *Table 2*. Another example of possible deviations between the predicted ROM results and those obtained by CFD is shown in *Figures 2e and 2f*, which indicate the maximum deflections for this geometry with m equal to 1.0. The comparison shows that the interaction of the mixed channel flow with the outlet edge at the air vent geometry is critical for the development and the deflection angle of the air jet. When the velocities in the upper edge area of the channel flow are overestimated by the reduced model approach, an increased deflection occurs. These are differences that can occur with the flow investigation methods shown. However, this comparison includes only a few parameter combinations. In order to provide a final accuracy analysis for the ROM approach, the entire parameter domain must be taken into account in a quantitative comparison.

The scalar target variables α and Δp are most important in terms of the evaluation and assessment of the individual air vent geometries. The quality of the prediction of these parameters was determined using the "coefficient of determination" R^2 based on a fivefold cross-validation. *Figure 3* shows the comparison of the predicted ROM results of both parameters using a fivefold cross-validation with the corresponding CFD observations as well as the corresponding R^2 value. For a perfect model prediction, all 200 data points in each plot would lie along the diagonal and the best possible R^2 value would be 1.0, corresponding to a perfect prediction of the target variables. ROM approaches with a value $R^2 \geq 0.8$ can be considered with a sufficient degree of accuracy [18]. According to the data set in *Figure 3a*, the R^2 value and the mean absolute error for the deflection angle α are 0.95 and 1.68° . The second value also agrees with the accuracy of the validation results from the preliminary study [14]. These deviations in the jet deflection angle range are considered as a good accuracy for a CFD solver in relation to an experiment. The corresponding R^2 value for the total pressure difference Δp in the system is 0.89 – based on the data points in *Figure 3b*. This value meets the required accuracy criterion stipulated in [19]. The mean absolute error for Δp is determined to be 13.0 Pa and initially this value appears to be higher than desirable. However, from the analysis of *Figure 3b*, it can be concluded that only 9% of the 200 data points have a relative deviation greater than $\pm 4\%$ compared to the CFD results. As described in the study of Ling et al. [9], due to the reduced order model, it must be noted that the accuracy is less favorable compared to the CFD simulation, especially in the boundary regions. Moreover, outliers may occur in the parameter domain, such as those shown in *Figure 3b*. The deviations which crop up in the boundary region of the parameter domain must be taken into account in the further analysis. Nevertheless, the method still shows a satisfactory accuracy. This means that the current accuracy of the ROM method is sufficiently established and can be used for further evaluations.

Results

This study focuses on the results of the analysis of the airflow predicted by the ROM and the conclusions regarding the influences of varying geometric and fluid mechanical parameters on the target parameters α and Δp . *Table 3* shows the minimum and maximum values of the flow parameters predicted by the ROM for the defined parameter domain indicated in *Table 1*. Further analyses are performed taking the

following base parameter values into account in order to make the changes understandable and to improve the resulting conclusions:

- base geometrical parameters:
 $h_3/h_1 = 1.0, l/h_1 = 1.0, h_4/h_1 = 1.0, \beta = 30^\circ$
- base flow-related parameters:
 $m = 1.0, \dot{V}_{total} = 60 \text{ m}^3\text{h}^{-1}$

Variation of the flow distribution m

Varying the volume flow distribution m results in an increase in the deflection angle α in the range from 0.5 to 1.0 considered for m . This is illustrated by the diagram in *Figure 4* along the left y -axis. Thus, the air vent geometry allows a linear adjustment of the airflow deflection angle as a function of the volume flow distribution, without a step-like hysteresis effect. It should be noted that this conclusion applies to the entire parameter domain, although *Figure 4* only shows the basic geometry. This representation and correspondence of the statements will be used throughout the remainder of this paper, unless further explicit specifications are made. In the example in *Figure 4*, the total pressure difference Δp varies in the range of 22.2 Pa and 35.3%. These resulting parameter values are plotted along the right y -axis in *Figure 4*. The decreasing values of this parameter can be explained by the mixing processes induced by the air vent geometry. In particular, flow processes for m smaller than 1.0 cause an increase in the total pressure difference in the system.

Variation of the total flow rate \dot{V}_{total}

The following results reflect the influence of the total flow rate \dot{V}_{total} , which varies in the range from 50 to 100 m^3h^{-1} . *Figure 5* shows the total flow rate \dot{V}_{total} as a function of the deflection angle α and the total pressure difference Δp for different flow distributions m . Due to the selected numerical flow boundary conditions, the result for the total pressure difference is as expected. The curves in *Figure 5a* show a significant increase in the target parameter α with an increasing total volume flow \dot{V}_{total} . Significant changes of up to $2.5^\circ / 10.7\%$ occur for $m = 0.75$ and up to $0.9^\circ / 8.2\%$ for α . These data indicate that with this air vent concept the total flow rate, \dot{V}_{total} , has an influence on the resulting flow direction, which in turn can be a disadvantage for the physical application. Adjusting the direction of the flow in the car cabin by changing the total volume flow is detrimental for the passenger comfort, as it can cause undesirable deflections. Nevertheless, the average deviation of 2.0° for the whole parameter domain indicated in *Table 1* remains within an acceptable range. Especially since a change of $\leq 2.5^\circ$ would not be noticeable to the passenger. Therefore, these deviations are not considered in the further analysis. The plots in *Figure 5b* show the expected increase in Δp with a rising flow rate for both flow distributions.

Variation of the outlet height ratio h_4/h_1

The first geometric parameter considers the variation of the outlet height ratio h_4/h_1 taking the defined range from 0.7 to 2.0 into account. A variation of the surface orientation β is included in the analysis of this parameter. *Figure 6* shows the deflection angle α (*Figure 6a*) and the total pressure difference Δp (*Figure 6b*) in relation to the outlet height ratio h_4/h_1 , taking a variation of the surface orientation β into account. *Figure 6a* illustrates the correlation for the parameter domain that the deflection angle α tends to increase as the outlet height ratio h_4/h_1 increases. The outlet height ratio h_4/h_1 depends on the orientation of the air outlet surface. Larger values of β result in greater flow deflection and thus to an increase in the deflection angle. Otherwise, as shown in *Figure 6b*, this results in an increasing total pressure

difference Δp . The reason for this is that a steeper orientation of the air inlet surface in the air vent geometry increases the flow deflection. Consequently, there is a trade-off with this geometric parameter, as improved flow deflection results in increased pressure losses. A further breakdown of this analysis is shown in *Figure 6a*, in a different progression of the lines for $\beta = 15^\circ$ and $\beta = 35^\circ$. The influence of the geometric parameter β is present, even if minimal, as the continuously increasing curve of the target variable α is always accompanied by an increasing outlet height ratio h_4/h_1 .

Variation of the separator distance ratio l/h_1

This study further analyzes the variation of the separator distance ratio l/h_1 in the defined range from 0.0 to 1.3, also taking into account variations in the surface orientation β and the outlet height ratio h_4/h_1 . The results show that a reduction in this geometric dimension leads to an increase in both the deflection angle α and the total pressure difference Δp . This effect is illustrated in the graphs of *Figure 7*. By increasing the parameter l/h_1 , the stagnation flow zone in the channel grows and a recirculation area can develop within the geometry. The airflow is deflected more significantly by the geometry interaction and the total pressure in the system decreases. There is also an influence of the separator distance ratio l/h_1 depending on the surface orientation β . As can be seen in *Figure 7a*, the gradient of the deflection angle α changes with varying β . Here, the deflection angle α is subject to a change of 23.0° at $\beta = 35^\circ$ along the varying separator distance ratio l/h_1 in the range from 0.0 to 1.3. At $\beta = 15^\circ$, the difference $\Delta\alpha$ is 3.3° . The effect of β on the separator distance ratio l/h_1 is therefore present. As the surface orientation β decreases, the influence of the varying separator distance ratio l/h_1 on the target parameters decreases as well. A similar behavior is observed for the outlet height ratio h_4/h_1 . *Figure 8a* shows that the slope of the line for $h_4/h_1 = 2.0$ is lower than the slope of the line for $h_4/h_1 = 0.8$. The orientation of the curves does not change in the graph. The influence of h_4 on l is also evident. Compared to the baseline geometry, an increase in the outlet height ratio h_4/h_1 leads to a reduction in the effect of the separator distance ratio l/h_1 . A similar behavior can also be seen for the total pressure difference Δp in *Figure 8b*.

Variation of the separator height ratio h_3/h_1

In the last part of the results section the variation of the separator height ratio h_3/h_1 in the range from 0.7 to 2.0 will be discussed, including variations of the air inlet separation distance ratio l/h_1 , the surface orientation β and the outlet height ratio h_4/h_1 . An increase in the separator height ratio h_3/h_1 results in a change in the deflection angle of up to 6.8° , see *Figure 9a*. A similar behavior to the geometric parameter h_4/h_1 is observed. In this case, an increase in the h_3/h_1 parameter is an attempt to lengthen the individual channels. As a result, the airflow is more uniformly guided by the geometry, which promotes flow deflection and the circulation across the air outlet. For the values indicated in *Figure 9b*, the changes in the total system pressure over the range of parameters are less than 6.5 Pa and therefore the influence can be considered minor. Consequently, this target parameter can be excluded from further analysis. *Figure 9a* shows a homogeneous distribution of the resulting lines as a function of the air inlet separator distance ratio l/h_1 . A variation of the separator height ratio h_3/h_1 including a variation of the air inlet separation distance ratio l/h_1 can thus be eliminated. This is also evident in *Figure 9b* for the total pressure difference Δp . *Figure 10* illustrates the significant influence of the surface orientation β on the first target parameter α and on the separator height ratio h_3/h_1 . It is evident that β has a greater influence on the direction of the jet than the separator height ratio. However, the influence of h_3 can be observed when it comes to the improved airflow

deflections. *Figure 11* shows a similarity in the distribution of line spacing compared to *Figure 6a*, indicating the influence of the outlet height ratio h_4/h_1 . The changes in the deflection angle α along the variation of the separator height ratio h_3/h_1 are smaller than 3%. This indicates that despite the variability of the separator height ratio, the influence on the deflection angle is comparatively small. Another observation is the influence of the outlet height ratio h_4/h_1 on the separator height ratio h_3/h_1 in relation to the deflection angle α . This is illustrated in *Figure 11* and underlines the complex interaction between the various geometric parameters and the target parameters of the system. These results provide insights into the optimization of flow systems and the control of the resulting air jet behavior.

Discussion

General Discussion

The following discussion illustrates the applicability of the ROM approach. The ability of the ROM to identify an optimal geometry within the defined parameter ranges (see *Table 1*), that combines both a high deflection angle α and a low total pressure difference Δp , is emphasized. To achieve this goal of defining the optimal geometry, the differential evolution method by Storn and Price [23] was used for optimization.

First of all, the design could be optimized from an aesthetic point of view. The outlet height h_4 reflects the visible area of the air vent concept. Since the parameter domain of the duct height h_1 is constant in this study, an exemplary requirement would be a maximum outlet height ratio of $h_4/h_1 \leq 1.0$ of the geometry. This requirement not only ensures harmonious integration of the air vent concept into the overall design, but also contributes to the aesthetic quality of the interior. The corresponding result domain of the target variables is shown in *Figure 12a*. The x -axis represents the deflection angle α and the y -axis shows the total pressure difference Δp . The coloring of the resulting areas are based on the outlet height ratio h_4/h_1 . If this optimization is also assigned a target value of 60 Pa from an energy efficiency point of view, the optimization can be found on the Pareto front in *Figure 12a*, marked with a light blue cross symbol. The resulting value for $\alpha = 27.5^\circ$ is also listed in *Table 4*. In terms of the requirements for a passenger air outlet in a car cabin [5,6], this is, however, not sufficient. Therefore, in this example, the limit for h_4/h_1 would have to be increased to 2.0 in the next optimization step. Based on *Table 4* and *Figure 12b* (gray star symbol) an improvement of α by 126% can be achieved. With a further relaxation of Δp to 100 Pa as the highest value, an additional 12% improvement for α (see white square symbol in *Figure 12b*) could be achieved for the deflection of the airflow. This example optimization loop demonstrates the power of the ROM approach. With an initial numerical effort all intermediate results can be determined, and thus individual optimization targets can be efficiently adapted and analyzed.

As another application example no geometric constraints were imposed, but a maximum total pressure difference Δp of 20 Pa was set as a flow-related limit. This optimization could be initiated by a car concept based on the technical aspect of energy efficiency. The aim is to find a suitable air vent geometry with maximum adjustment possibilities for the jet with a limited pressure loss balance. The results are presented in *Figure 13*, which shows a section of the mean air velocity contour plot in the x - y -plane for the optimal geometry as predicted by the ROM. This contour plot clearly illustrates the optimal flow characteristics for the considered flow system with the resulting target parameters of $\alpha = 38^\circ$ and $\Delta p = 20$ Pa (see gray circle symbol in *Figure 12b*). From the geometric parameters depicted in *Figure 13*, it can be seen that h_4/h_1 is at the limit of the defined ranges of *Table 1*. Considering the previous results and this optimization, an extension of

the parameter domain, e.g., in terms of h_4/h_1 , could lead to even better results for the energy optimized air vent.

Prototyping and testing of an optimal geometry

The parameter domain considered in the study is limited compared to reality as neither blades nor guide elements nor external obstacles were taken into account. In order to illustrate the applicability and the limitations of the ROM method using a basic model for the automotive development process, the optimized geometry shown in *Figure 13* is transferred to a realistic prototype. The simplified 2D geometry was constructed with a width of $100h_1$ to form a complete air outlet with adjustable guiding elements (see *Figure 14a*) that allow the jet to be aligned in the neutral position ($m = 0.5$) and the maximum position ($m = 1.0$). This geometry was produced by 3D printing and used for an experimental investigation (see *Figure 14b*). A constant, defined volume flow \dot{V}_{total} of $60 \text{ m}^3\text{h}^{-1}$ was set on the explicit air vent test bench. The static pressure difference Δp_{static} upstream of the air outlet was determined by means of small holes in the duct wall, which were connected to a pressure transmitter via a tube. The experimental results of the test bench are compared with CFD simulations. The numerical 3D model (see *Figure 14c*) considers the air vent in isolation and in a free environment without additional obstacles or nearby walls, analogous to the test bench. The numerical setup corresponds to the preliminary study by Ullrich et al. [14]. The CFD model of the isolated air outlet was meshed with 7.1 million cells. The comparatively low number of 0.4 million cells for the ROM model clearly shows the significant additional effort required for the final 3D calculations. The first comparison relates to the mean air velocity along the main flow direction of the jet, which results from the optimized geometry (*Figure 13*). The predicted ROM velocity values are compared with the experimental measurements shown in *Figure 15*. It is evident that the ROM overestimates the mean air velocities compared to reality, which can be attributed to the idealized assumptions of the model and the non-consideration of 3D flow effects. Nevertheless, the model provides indicative results with a smaller computational effort. The experimental measurements agree with the CFD air vent results with a mean deviation of $0.28 \text{ ms}^{-1} / 8.3\%$. The diagram confirms the validation of the preliminary study [14]. Another key quantity to be compared is the pressure loss of the optimized geometry, which is shown in *Figure 16* due to the experimental measurement based on the static pressure difference Δp_{static} . As already shown in *Figure 5b*, the deflection of the airflow leads to an increase in the pressure loss in the system. The integration of air guiding elements and the consideration of 3D flow effects increases the static pressure upstream of the air outlet. This offset would have to be taken into account in a possible development process, but the results are convincing with a trend-setting statement. The results of the CFD air vent model deviate from the experimental data by a maximum of $2.6 \text{ Pa} / 7.7\%$.

Application in a car cabin

Finally, the optimized air vent configuration based on the ROM analysis shown in *Figure 13* was implemented in a full car cabin using 3D CFD analysis tools. This model included the curved ducts in front of the new air vents, which connect the outlet geometry with the heat, ventilation and air conditioning (HVAC) system in the engine compartment. The second numerical 3D model (see *Figure 14d*), which simulates the air of the outlet geometry in the ventilation system of an exemplary car cabin, was meshed with 59.7 million cells and the setup was derived from the preliminary study [14]. For the evaluation, the average air velocity (see *Figure 15*), the maximum deflection angles as well as the static pressure difference (see *Figure 16*) were determined for the jet from the center air vent. The results reveal that

additional effects, such as recirculation and obstacles in the far field, occur within the car cabin and influence the airflow. This results in deviations in the mean air velocity in the range $xh_1^{-1} > 2.5$ in *Figure 15*. The present study focuses on the deflection angle α of the jet. In the CFD car cabin results, the deflection occurs at an angle α of 36° upwards and -34° downwards, which shows a deviation of 5.3% and 10.5%, respectively, from the estimated ROM value of $\pm 38^\circ$. The different upward and downward alignment of the jet results from the curved air ducts behind the dashboard of the car. This prevents a uniform volume flow over the height of the duct in front of the air vent. The values for α show that the simplified 2D model is also suitable for predicting the flow direction to some degree. However, the differences in mean air velocities also indicate that the ROM model would need to be extended to the significantly larger 3D CFD model of the car cabin if detailed thermal comfort parameters, such as drafts on the passenger, are to be evaluated for an optimal outlet geometry. The deviations in the results of the CFD car cabin model for Δp_{static} (see *Figure 16*) can again be attributed to the complexity of the entire ventilation system and the volume flow distribution within the air ducts. The ability to extend the model to 3D car models also offers the potential of considering target variables, such as thermal comfort and jet impact, to further optimize air deflection, efficiency and overall comfort in the car cabin.

Conclusions

In summary, it can be said that the conducted analysis of the influence of geometric and fluid mechanical parameters, in particular the dimensions of the air outlet, provides important insights into the evolution of the deflection angles and the total pressure differences in the system. The application of the toolchain for an air vent concept based on CFD and ROM was able to show a complete result space. Variations in parameters, such as the air vent surface orientation β , the outlet height h_4 , the separator distance l and the separator height h_3 lead to different effects on the airflow behavior. In particular, changes in the surface orientation β always correlate with an increase in the deflection angle α and the total pressure difference Δp , highlighting their significant impact on system performance. In contrast, variations in the outlet height ratio h_4 influence the deflection angle α and total pressure difference Δp in a positive sense in terms of the air vent geometry requirements. In addition, the study examines the interaction of the geometric parameters and shows complex interactions that influence the flow behavior. While certain parameters show clear dependencies, others exhibit more complex interactions. With this comprehensive understanding of the influence of geometric parameters on flow characteristics, new and innovative air vent concepts can be developed and implemented. By balancing design considerations and technical requirements, optimal solutions can be achieved. In the future, this research will provide the basis for modeling and implementing innovative air vent concepts designed to meet specific application requirements. By identifying optimal geometries within defined parameter ranges and constraints, it will be possible to achieve high deflection angles (α) while minimizing overall pressure differences (Δp) to improve the overall system performance and efficiency.

References

1. Schaut, S. and Sawodny, O., "Thermal management for the cabin of a battery electric vehicle considering passengers' comfort", *IEEE Transactions on Control Systems Technology* 28(4):1476-1492, 2020.
2. Karlsson, B. S. A. and Aronsson, N. and Svensson, K. A., "Using semantic environment description as a tool to evaluate car interiors", *Ergonomics* 46(13/14): 1408–1422, 2003.
3. Baker, P. J. and Jenkins, M. and Wagner, S. and Ellinger, M., "An Optimised Thermal Design and Development Process for Passenger Compartments of Vehicles", EASC 2009, 4th European Automotive Simulation Conference, July 6-7, Munich, Germany, 2009.
4. A2Mac1 Automotive benchmarking, accessed Januar 2024, <https://www.a2mac1.com/>.
5. Ležovič, T. and Lízal, F. and Jedelský, J. and Jícha, M., "HVAC automotive vents evaluation and their performance", *HVAC&R Research* 19(8):1073-1082, 2013.
6. Lízal, F. and Pech, O. and Jedelský, J. and Tuhovčák, J. and Jícha, M., "The automotive ventilation test case: Investigation of the velocity field downstream of a benchmark vent using smoke visualization and hot-wire anemometry", *Proceedings of the Institution of Mechanical Engineers, Part D: Journal of Automobile Engineering* 233(8):2146-2160, 2019.
7. Yada, N and Ito, Y., Patent No.: JPS 62 228833 A2, Japan Patent Office, 1987.
8. Othmer, C., Patent No.: DE 10 2018 203 076 A1, German Patent and Trade Mark Office, 2019.
9. Ling, J. and Aute, V. and Hwang, Y. and Radermacher, R., "A New Computational Tool for Automotive Cabin Air Temperature Simulation", *SAE Int. J. Passeng. Cars - Mech. Syst.* 6(2):841-846, 2013.
10. Wei, Y. and Zhang, T. and Wang, S., "Prompt design of the air-supply opening size for a commercial airplane based on the proper orthogonal decomposition of flows", *Building and Environment* 96:131-141, 2016.
11. Wei, Y. and Liu, W. and Xue, Y. and Zhai, Z. and Chen, Q. and Zhang, T., "Inverse design of aircraft cabin ventilation by integrating three methods", *Building and Environment* 150:33-43, 2019.
12. Christ, P. and Sattelmayer, R., "Reduced Order Modelling of Flow and Mixing in an Automobile HVAC System Using Proper Orthogonal Decomposition", *Applied Thermal Engineering* 133:211-223, 2018.
13. Mrosek, M. and Othmer, C. and Radespiel, R., "Reduced-Order Modeling of Vehicle Aerodynamics via Proper Orthogonal Decomposition", *SAE Int. J. Passeng. Cars – Mech. Syst.* 12(3):225-236, 2019.
14. Ullrich, S. and Buder, R. and Boughanmi, N. and Friebe, C. and Wagner, C., "Numerical Study of the Airflow Distribution in a Passenger Car Cabin Validated with PIV", *New Results in Numerical and Experimental Fluid Mechanics XII. Notes on Numerical Fluid Mechanics and Multidisciplinary Design*, Springer 142:457-467, 2020.
15. Heider, A. and Konstantinov, M. and Lauenroth, G. and Rütten, M. and Werner, F. and Wagner, C., "Experimental and numerical investigations of cabinflow in a mini-van", *Aerodynamics of Heavy Vehicles III: Trucks, Buses and Trains*, 2010. <https://elib.dlr.de/67185/>
16. You, R. and Chen, J. and Shi, Z. and Liu, W. and Lin, C.-H. and Wei, D. and Chen, Q., "Experimental and numerical study of airflow distribution in an aircraft cabin mock-up with a gasper on", *Journal of Building Performance Simulation* 9(5): 555-566, 2016.
17. Jaramillo, J.E. and Pérez-Segarra, C.D. and Rodriguez, I. and Oliva, A. "Numerical study of plane and round impinging jets using rans models", *Numerical Heat Transfer, Part B: Fundamentals*, 54:213–237, 2008.
18. Braconnier, T. and Ferrier, M. and Jouhaud, J.-C. and Montagnac, M. et al., "Towards an Adaptive POD/SVD Surrogate Model for Aeronautic Design", *Computers & Fluids* 40(1):195-209, 2011.
19. Forrester, A. and Söbester, A. and Keane, A., "Engineering Design via Surrogate Modelling: A Practical Guide", Chichester: Wiley, 2008.
20. Xiao, M. and Breikopf, P. and Filomeno Coelho, R. and Knopf-Lenoir, C. et al., "Model Reduction by CPOD and Kriging", *Structural and Multidisciplinary Optimization* 41(4):555-574, 2010.
21. Fossati, M. and Habashi, W., "Multiparameter Analysis of Aero-Icing Problems Using Proper Orthogonal Decomposition and Multidimensional Interpolation", *AIAA Journal* 51(4):946-960, 2013.
22. Karcher, N. "POD-Based Model-Order Reduction for Discontinuous Parameters", *Fluids* 7(242), 2022.
23. Storn, R. and Price, K., "Differential Evolution - A Simple and Efficient Heuristic for Global Optimization over Continuous Spaces", *Journal of Global Optimization* 11:341-359, 1997.

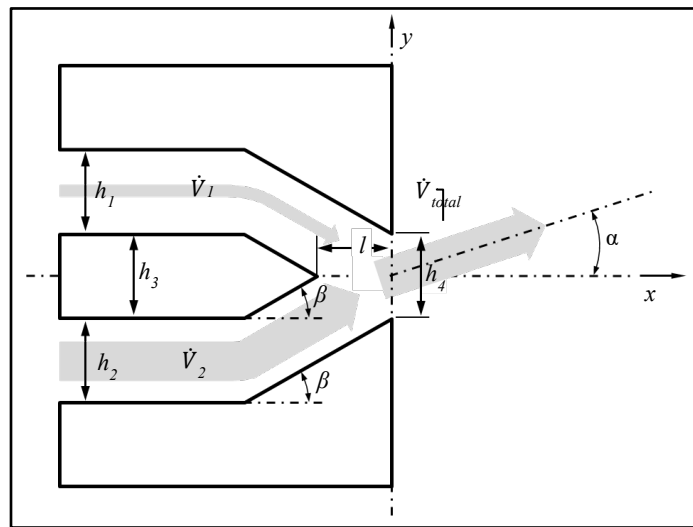
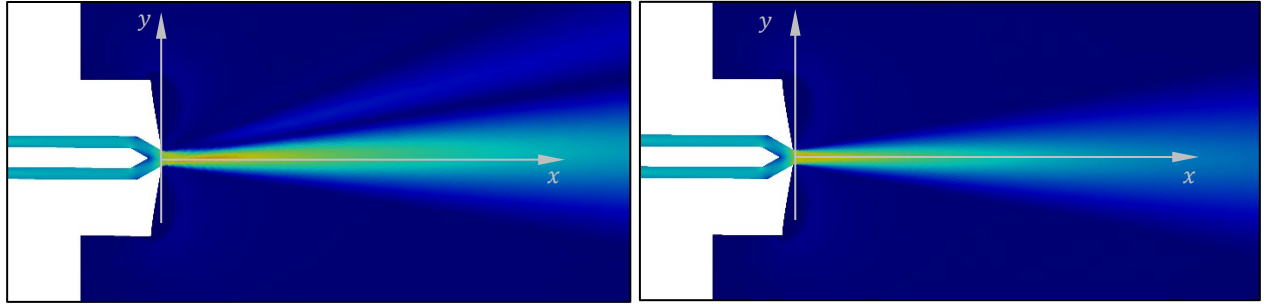


Figure 1: Schematic and geometric parameters of the air vent.

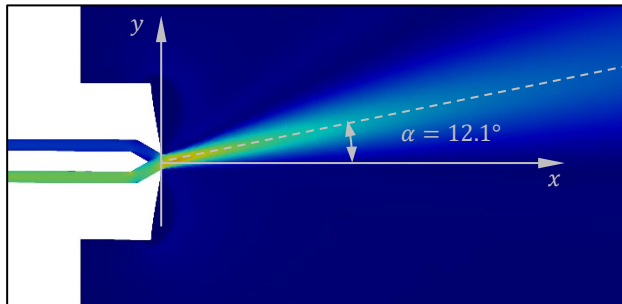
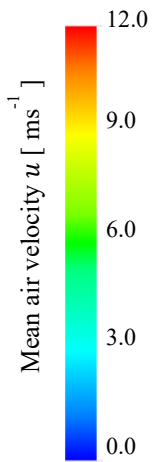
Table 1: Minimum and maximum values of the defined parameter domain for the air outlet.

Modified parameter	Unit	Minimum	Maximum
Separator height ratio h_3/h_1	[-]	0.7	2.0
Separator distance ratio l/h_1	[-]	0.0	1.3
Outlet height ratio h_4/h_1	[-]	0.7	2.0
Surface orientation β	[°]	15.0	60.0
Flow distribution m	[-]	0.5	1.0
Total flow rate \dot{V}_{total}	[m ³ h ⁻¹]	50.0	100.0

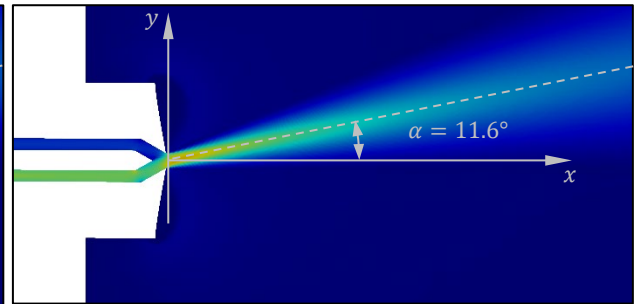


(a) ROM result for $m = 0.50$

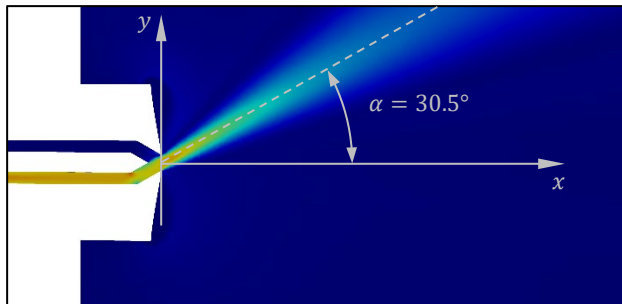
(b) CFD result for $m = 0.50$



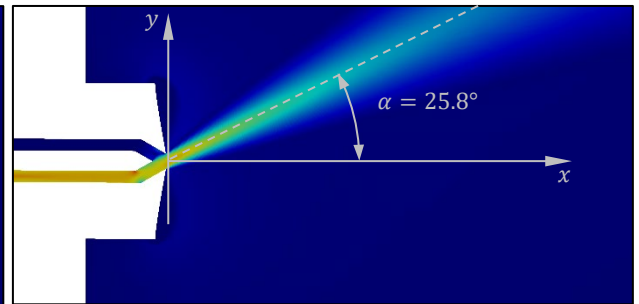
(c) ROM result for $m = 0.75$



(d) CFD result for $m = 0.75$



(e) ROM result for $m = 1.00$

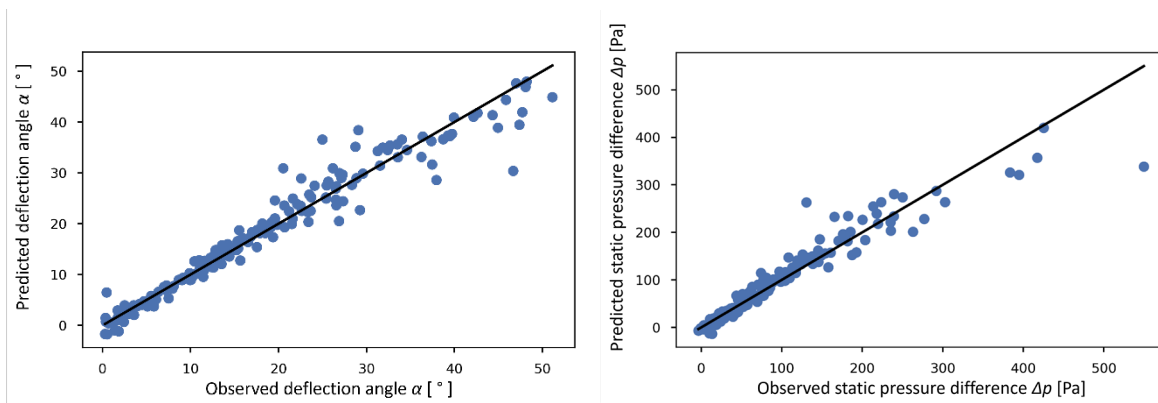


(f) CFD result for $m = 1.00$

Figure 2: Section of the mean air velocity contour plot in the x - y -plane predicted by the Reduced Order Model, (a), (c) and (e), and obtained via Computational Fluid Dynamics, (b), (d) and (f), for different flow distributions m . Geometric parameter: $h_3/h_1 = 1.71$, $l/h_1 = 1.16$, $h_4/h_1 = 1.30$, $\beta = 29.24^\circ$. Flow-related parameter: $\dot{V}_{total} = 64 \text{ m}^3\text{h}^{-1}$.

Table 2: Results of the resulting flow parameters predicted by the ROM and observed by the numerical calculation for the configurations in Figure 2.

Flow distribution	$m = 0.50$		$m = 0.75$		$m = 1.00$	
Resulting flow parameter	α [°]	Δp [Pa]	α [°]	Δp [Pa]	α [°]	Δp [Pa]
Predicted results [ROM]	-0.07	40.53	12.16	38.63	30.52	37.04
Observed results [CFD]	0.25	35.43	11.55	37.69	25.84	37.29
Difference	0.32	-5.10	-0.61	-0.94	-4.68	0.25



(a) Deflection angle α

(b) Total pressure difference Δp

Figure 3: Correlation plots for the 200 predicted (ROM) and the observed (CFD) deflection angles α , Figure (a), and total pressure differences Δp , Figure (b), resulting from the fivefold cross-validation. In a faultless model prediction, all data points in the respective diagram would be located along the diagonal line.

Table 3: Minimum and maximum values of the resulting flow parameters predicted by the ROM for the defined parameter domain indicated in Table 1.

Resulting flow parameter	Unit	Minimum	Maximum
Reynolds-number Re	[-]	3.6×10^3	2.3×10^4
Deflection angle α	[°]	-5.5	72.1
Total pressure diff. Δp	[Pa]	13.7	729.9

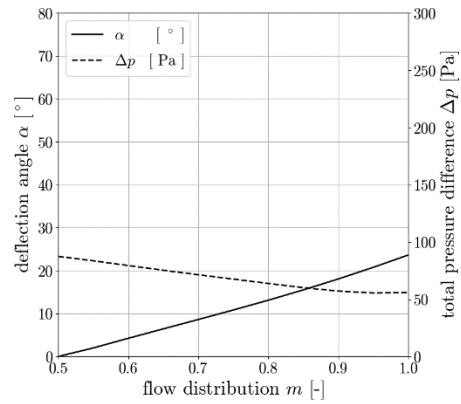
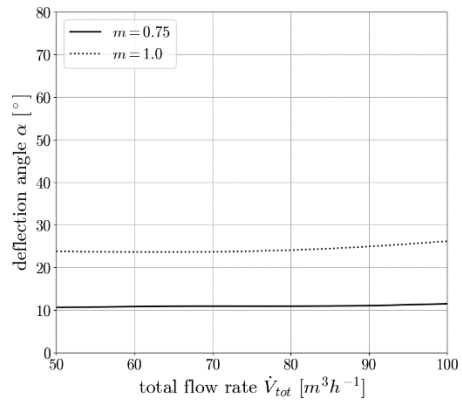


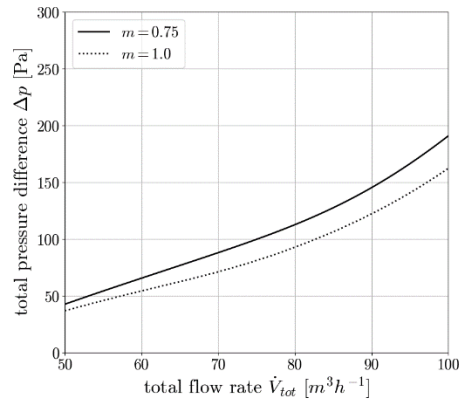
Figure 4: Flow distribution m with respect to the deflection angle α as well as the total pressure difference Δp .

Constant geometrical parameters: $h_3/h_1 = 1.0$, $l/h_1 = 1.0$, $h_4/h_1 = 1.0$, $\beta = 30^\circ$.

Constant flow-related parameter: $\dot{V}_{total} = 60 \text{ m}^3\text{h}^{-1}$.



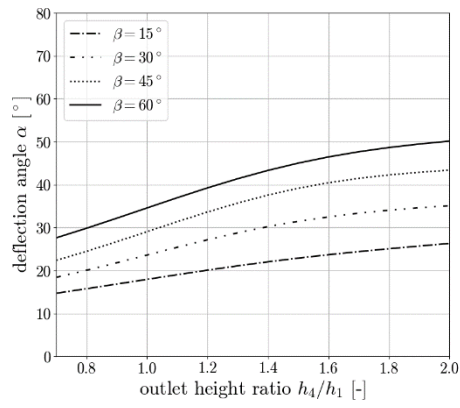
(a) Deflection angle α



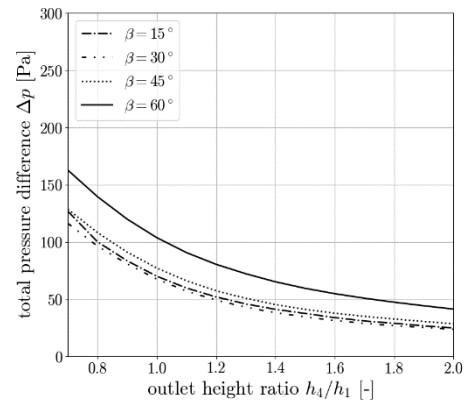
(b) Total pressure difference Δp

Figure 5: Total flow rate \dot{V}_{total} with respect to the deflection angle α (a) and the total pressure difference Δp (b) including a variation of the flow distributions m .

Constant geometrical parameters: $h_3/h_1 = 1.0$, $l/h_1 = 1.0$, $h_4/h_1 = 1.0$, $\beta = 30^\circ$.



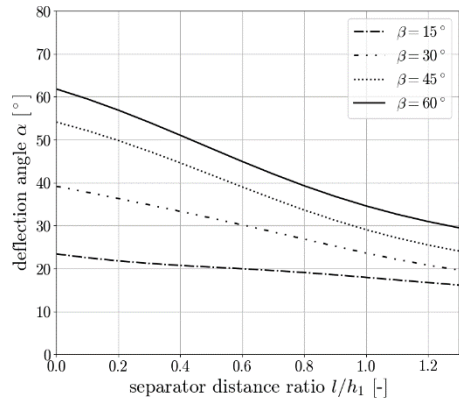
(a) Deflection angle α



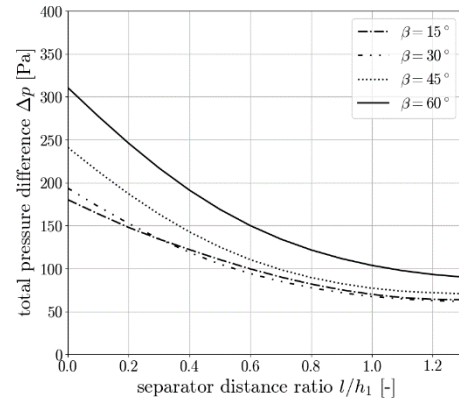
(b) Total pressure difference Δp

Figure 6: Air vent height ratio h_4/h_1 with respect to the deflection angle α (a) and the total pressure difference Δp (b) including a variation of the air vent surface orientation β .

Constant geometrical parameters: $h_3/h_1 = 1.0$, $l/h_1 = 1.0$.
 Constant flow-related parameters: $m = 1.0$, $\dot{V}_{total} = 60 \text{ m}^3\text{h}^{-1}$.



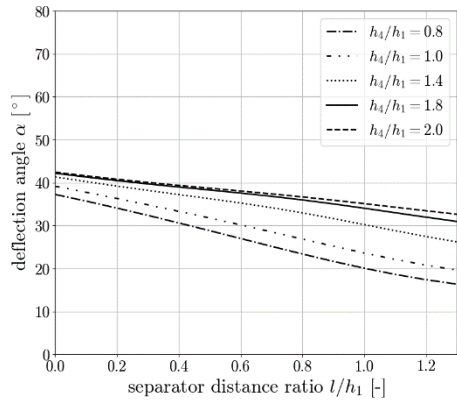
(a) Deflection angle α



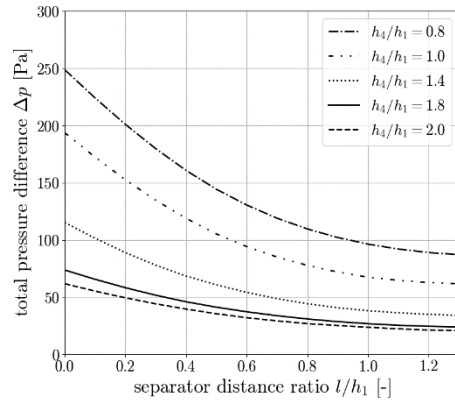
(b) Total pressure difference Δp

Figure 7: Air vent separator distance ratio l/h_1 with respect to the deflection angle α (a) and the total pressure difference Δp (b) including a variation of the air vent surface orientation β .

Constant geometrical parameters: $h_3/h_1 = 1.0$, $h_4/h_1 = 1.0$.
 Constant flow-related parameters: $m = 1.0$, $\dot{V}_{total} = 60 \text{ m}^3\text{h}^{-1}$.



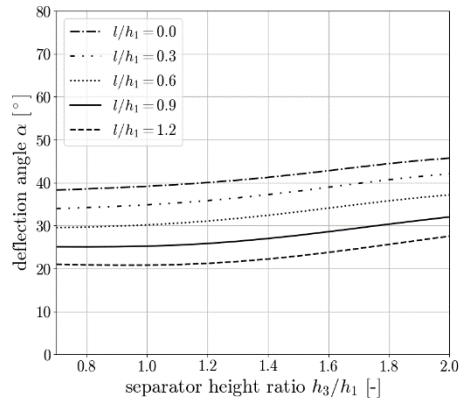
(a) Deflection angle α



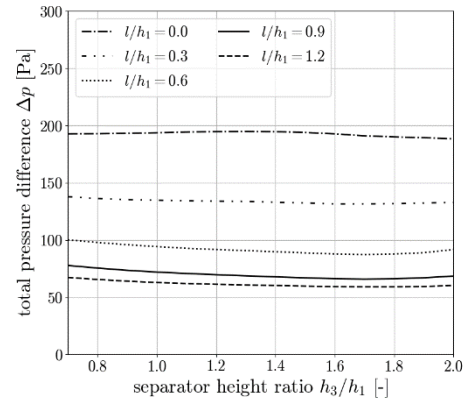
(b) Total pressure difference Δp

Figure 8: Air vent separator distance ratio l/h_1 with respect to the deflection angle α (a) and the total pressure difference Δp (b) including a variation of the air vent height ratio h_4/h_1 .

Constant geometrical parameters: $h_3/h_1 = 1.0$, $\beta = 30^\circ$.
 Constant flow-related parameters: $m = 1.0$, $\dot{V}_{total} = 60 \text{ m}^3\text{h}^{-1}$.



(a) Deflection angle α



(b) Total pressure difference Δp

Figure 9: Air vent separator height ratio h_3/h_1 with respect to the deflection angle α (a) and the total pressure difference Δp (b) including a variation of the air vent separator distance ratio l/h_1 .

Constant geometrical parameters: $h_4/h_1 = 1.0$, $\beta = 30^\circ$.
 Constant flow-related parameters: $m = 1.0$, $\dot{V}_{total} = 60 \text{ m}^3\text{h}^{-1}$.

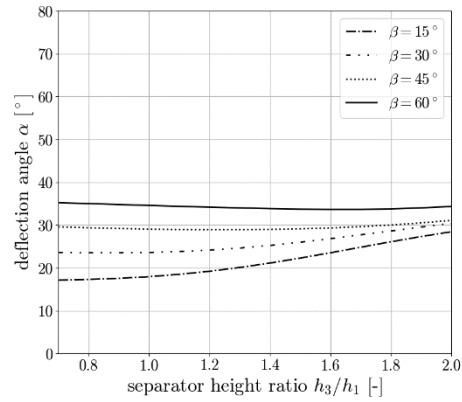


Figure 10: Air vent separator height ratio h_3/h_1 with respect to the deflection angle α including a variation of the air vent surface orientation β .

Constant geometrical parameters: $l/h_1 = 1.0$, $h_4/h_1 = 1.0$.
 Constant flow-related parameters: $m = 1.0$, $\dot{V}_{total} = 60 \text{ m}^3\text{h}^{-1}$.

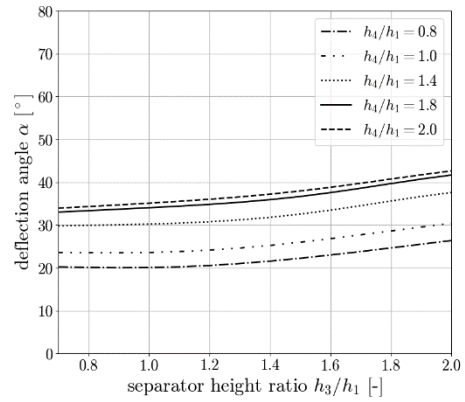
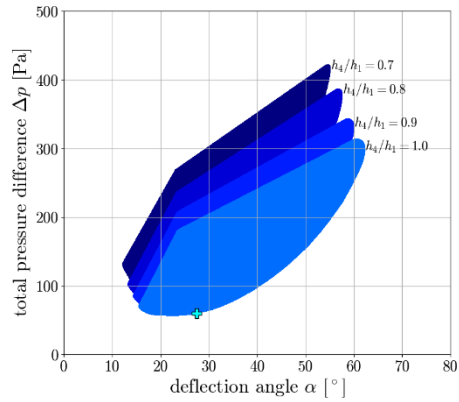
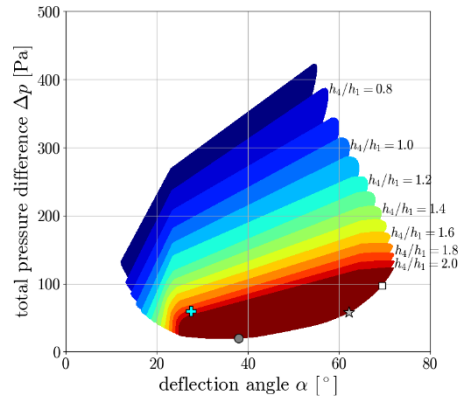


Figure 11: Air vent separator height ratio h_3/h_1 with respect to the deflection angle α including a variation of the air vent height ratio h_4/h_1 .

Constant geometrical parameters: $l/h_1 = 1.0$, $\beta = 30^\circ$.
 Constant flow-related parameters: $m = 1.0$, $\dot{V}_{total} = 60 \text{ m}^3\text{h}^{-1}$.



(a) Geometrical limit: $h_4/h_1 \leq 1.0$







(b) Without geometrical limit

Figure 12: The deflection angle α with respect to the total pressure difference Δp predicted by the Reduced Order Model for all geometry parameters including different optimization results due to various restrictions in Table 4. Color-coded by the air vent height ratio h_4/h_1 .

Constant flow-related parameters: $m = 1.0$, $\dot{V}_{total} = 60 \text{ m}^3\text{h}^{-1}$.

Table 4: Different optimization results with regard to the deflection angle α caused by various restrictions.

Geometrical limit h_2/h_1	Target parameter limit Δp	Optimum target parameter α	Data point in Figure 13
1.0	60 Pa	27.5°	
2.0	60 Pa	62.2°	
2.0	100 Pa	69.4°	
no limit	20 Pa	37.8°	

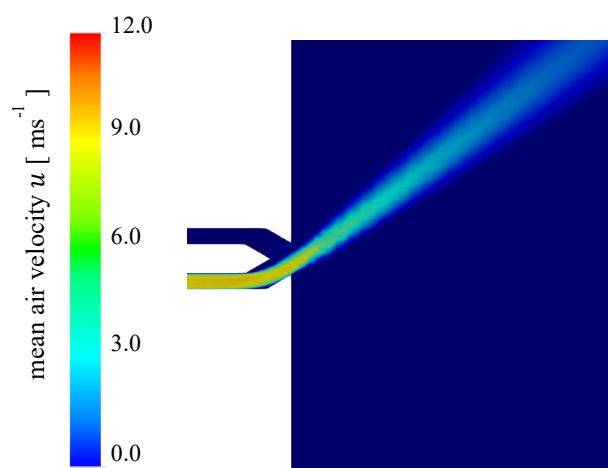
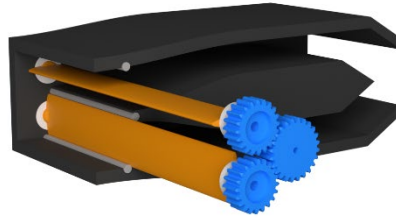


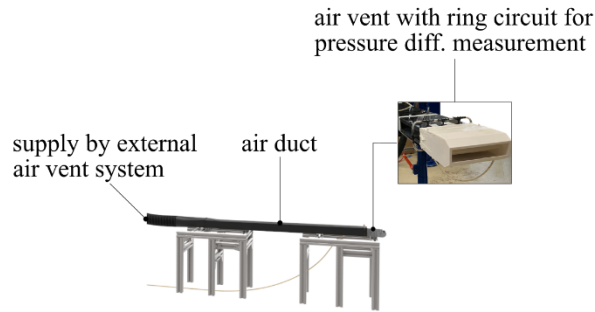
Figure 13: Section of the 2D mean air velocity contour plot in the x - y -plane predicted by the Reduced Order Model for the optimal geometry.

Geometrical parameters: $h_3/h_1 = 1.8$, $l/h_1 = 1.3$, $h_4/h_1 = 2.0$, $\beta = 30^\circ$.

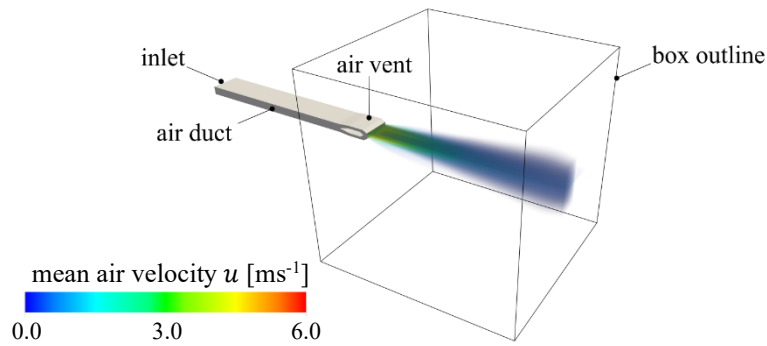
Flow-related parameters: $m = 1.0$, $\dot{V}_{total} = 60 \text{ m}^3\text{h}^{-1}$.



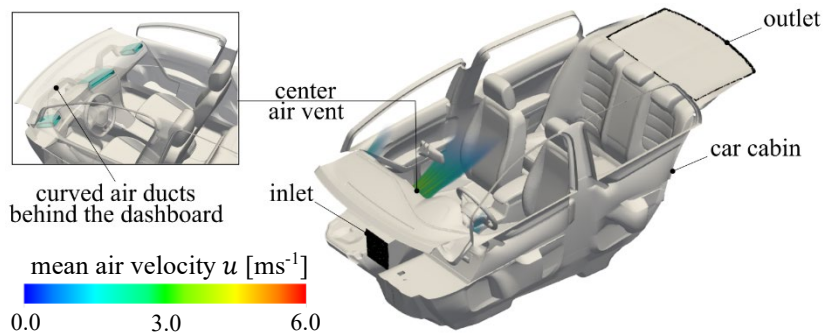
(a) Air outlet prototype with adjustable guiding elements ($m = 1.0$)



(b) Experimental measurement



(c) 3D CFD air vent



(d) 3D CFD car cabin

Figure 14: Schematic representation of the additional flow investigation of the jet resulting from the air outlet prototype with adjustable guiding elements (a). Experimental measurement of the jet from a single air vent integrated in an airflow test bench in free environment (b), numerical 3D flow analysis of the air vent in free environment (c) and integrated in an exemplary car cabin (d).

Geometrical parameters of the air vent: $h_3/h_1 = 1.8$, $l/h_1 = 1.3$, $h_4/h_1 = 2.0$, $\beta = 30^\circ$, $\text{width}/h_1 = 100$.

Flow-related parameters: $m = 0.50$, $\dot{V}_{\text{total}} = 60 \text{ m}^3\text{h}^{-1}$.

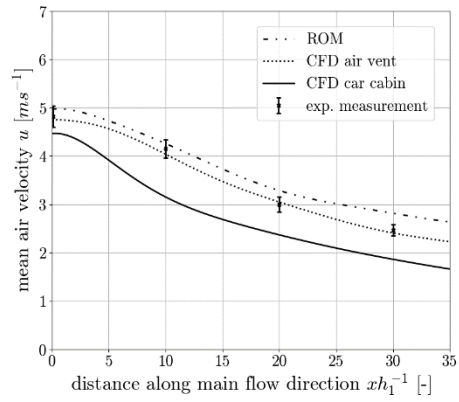


Figure 15: Mean air velocity along the main flow direction of the jet resulting from the optimized geometry. Results predicted with the Reduced Order Model compared to the respective analysis methods shown in Figure 14.

Flow-related parameters: $m = 0.50$, $\dot{V}_{total} = 60 \text{ m}^3\text{h}^{-1}$.

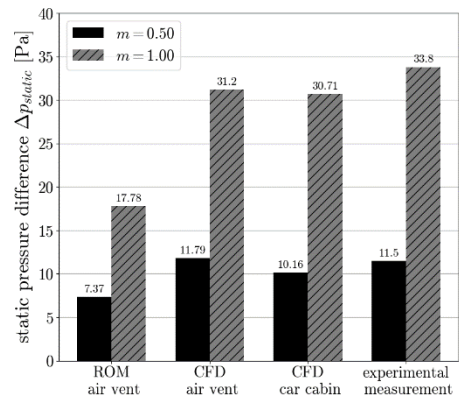


Figure 16: Static pressure difference of the optimized air vent geometry for two flow distributions m estimated by the Reduced Order Model compared to the different analysis methods shown in Figure 14.

Flow-related parameter: $\dot{V}_{total} = 60 \text{ m}^3\text{h}^{-1}$.